Characterization of Petroleum Deposits Formed in a Producing Well by Synchrotron Radiation-Based Microanalyses

E. Chouparova[†]
Laboratory for Earth and Environmental Sciences, Brookhaven National Laboratory, Upton, New York 11973-5000
A. Lanzirotti
Consortium for Advanced Radiation Sources, The University of Chicago, Chicago, Illinois 60637
H. Feng[‡] and K. W. Jones*
Laboratory for Earth and Environmental Sciences, Brookhaven National Laboratory, Upton, New York 11973-5000
N. Marinkovic
Albert Einstein College of Medicine, Bronx, New York 10461
C. Whitson[§]
Petroleum Engineering Department, University of Oklahoma, Norman, Oklahoma 73017
P. Philp
School of Geology and Geophysics, University of Oklahoma, Norman, Oklahoma 73019

Received May 6, 2003. Revised Manuscript Received April 13, 2004

Tubing strings in producing oil wells are often blocked by solid or semisolid deposits that necessitate costly remedial actions to maintain production. We describe here results obtained by a set of synchrotron radiation-based microanalytical techniques to investigate depth profiles and heterogeneity of organic compounds and metals in a series of deposit samples formed at different depths in blocked tubing strings from an operational oil well. Micrometer-scale synchrotron Fourier transform infrared (FTIR) spectroscopic and X-ray fluorescence (XRF) analyses using facilities at the National Synchrotron Light Source at Brookhaven National Laboratory are presented. Visualization, compositional mapping, high-resolution, and nondestructive analysis of samples are some of the main advantages of applying synchrotron-based microanalytical techniques. The results indicate that the depth profile of deposits formed along the same well varies and is characterized by the following main trends from deeper to shallower samples: (1) amount of deposits increases, a complete tubing plugging occurs at shallower levels; (2) concentration of inorganic components decreases; (3) sulfur-containing compounds in the deposits shift relative abundances from predominantly reduced to predominantly oxidized forms; (4) carbon content and H/C atomic ratio increase, S/C and N/C atomic ratios decrease; (5) higher molecular weight (HMW) *n*-alkane mixtures (wax components) shift the maximum of their distribution from higher to lower molecular weight mixtures; (6) maximum concentrations of some elements (V, Ba, Ti, and Cr) are found in the deepest samples; (7) elements present in all samples along the depth profile are Ca, Fe, Ni, Cu, Pb, and Br. Three different types of aggregates (10−60 μm) dominated by nonpolar, polar, and mixed polar/nonpolar compounds are identified in the same deposit. Predominantly nonpolar (Type I) aggregates contain long chain alkanes, aromatic compounds, and aliphatic thiols, consistent with the characteristics of "wax" type aggregates. The presence of carboxylic acids distributed irregularly toward the periphery of a FTIR mapped aggregate of this type is indicated. Predominantly polar (Type II) aggregates consist of aromatic structures, sulfur, nitrogen, and oxygen-containing compounds, some aliphatic structures, and water molecules possibly associated with salts. The characteristics of this type of aggregates are consistent with "asphaltene" type aggregates. This type of aggregate is found associated with inorganic (probably carbonate, clay, and/or corrosion) particles. Aggregates with mixed nonpolar/polar character are also observed, indicating possible adsorption of resins and asphaltenes by high molecular weight hydrocarbons. Depth profiles show heterogeneity in metal distribution, most likely reflecting systematic changes in proportions between the metal concentrations associated with the organic and inorganic phases in the deposits. Spatial heterogeneity in metals distribution is found on a scale of a hundred micrometers within the same sample. The study demonstrates the benefits of applying a set of complementary synchrotron-based microanalytical nondestructive methods for characterization of the deposits. The results demonstrate the suitability of the methods for studying organic solid aggregation and petroleum deposition problems, as well as the potential for testing and developing chemical and microbial methods for solid petroleum deposit remediation.

Introduction

An ongoing issue in petroleum production is equipment blockage by solid or semisolid deposits that can significantly lower productivity. Such events often necessitate costly remedial actions in order to keep these wells producing. As an example, a plugging with solid−semisolid deposit material occurred in the tubing strings of the oil-producing well Mosteller 1 in Oklahoma. This caused production to be stopped and remediation operations to be performed. The remediation operations involved pulling to the surface the well tubing strings (rods), with a total length exceeding 2743 m, and then cleaning the plugged strings. Such operations are very

* Corresponding author. E-mail: jones@bnl.gov.
[†] Present address: Shell Exploration and Production Technology and Research, Bellaire Technology Center, Houston, TX 77025.
[‡] Present address: Department of Earth and Environmental Studies, Montclair State University, Upper Montclair, NJ 07043.
[§] Present address: Department of Petroleum Engineering and Applied Geophysics, Norwegian Institute of Technology, 7034 Trondheim, Norway.

10.1021/ef030108a CCC: $27.50
Published on Web 07/03/2004

costly with respect to both the cost of the remediation and the time of lost petroleum production.

The material that reduces tubing diameter or plugs petroleum well equipment is known to represent a complex mixture of hydrocarbon (wax) and non-hydrocarbon (resins and asphaltenes) fractions, along with additional trapped oil, water, and inorganic material in various proportions.[1,2] The amount and composition of the deposits are a function of changing temperature, pressure, and oil composition during production.[3−9] As a result of these changing conditions, heavy components with different chemical composition and properties that are dissolved and/or dispersed in the oil can reach supersaturation and begin to crystallize, aggregate, and accumulate, often around already existing nuclei. Asphaltene and fine inorganic particles (e.g., rock, mineral, and/or corrosion particles) can act as such nuclei, even though asphaltenes can also act as natural dispersants for the wax crystals.[10−13]

The petroleum-derived solid deposits are often referred to in the literature as "paraffin (wax)" or "asphaltene" deposits, even though they represent a complex mixture with variable compositions and properties. Petroleum wax by definition is a fraction of petroleum dominated by straight chain alkanes that are solid at ambient temperature (i.e., above *n*-C_{18}) with smaller amounts of isoalkanes, cycloalkanes, and aromatics.[1,14,15] Petroleum waxes are commonly classified as macrocrystalline (paraffin), intermediate, and microcrystalline (amorphous) types.[11,15] Macrocrystalline waxes consist of lower molecular weight range (LMW) *n*-alkanes (C_{18}−C_{30}) with melting points in the range of 40−60 °C, while the microcrystalline waxes are dominated by the higher molecular weight (HMW) alkanes (above C_{30}−C_{50}) and have much higher melting point ranges (above 60−90 °C).[16] Thus, the HMW hydrocarbons (microcrystalline waxes) would be the first to precipitate under decreasing temperature conditions. Only about a decade ago it was recognized and demonstrated that deposits formed in well equipment and pipelines often have concentrated abundances of high molecular weight *n*-alkane mixtures that otherwise could hardly be detected in the produced whole oil.[17−21] One of the earliest studies on "rod wax" deposits has shown the coexistence of "waxes, resins and gums, and asphalt material."[1] Four rod waxes were reported to consist of 75 to 82% wax, 15 to 21% resin, and up to 3% asphaltene (obtained as a fraction insoluble in both petroleum ether and hot acetone). The presence of resins in the waxes was attributed to similar solubility properties and to absorption of resins by waxes during the crystallization process. Coprecipitation of resins, asphaltenes, and hydrocarbons is commonly observed when using routine laboratory asphaltene precipitation procedures with an excess of light hydrocarbon solvents.[22] The possibility of adsorption of resins and asphaltenes with the HMW hydrocarbons resulting in their coprecipitation has been discussed in several studies.[12,13,23] These observations could be related to the much more similar melting point ranges, solubility, and adhesive properties of HMW hydrocarbon mixtures (microcrystalline waxes) to resins and asphaltenes than to macro-crystalline waxes (LMW hydrocarbons). However, the type and properties of aggregates formed by the association between HMW alkanes, resins, and asphaltenes are not completely clear. It is not clear, for example, if the HMW hydrocarbons are occluded in the resin−asphaltene matrix, or if resin−asphaltenes are trapped as occlusions during wax crystallization, or if both types of aggregates may be formed under different conditions.

Wax deposition is governed by liquid−solid phase transitions of alkane mixtures and is strongly influenced by reduction in temperature and decrease in solubility of heavy hydrocarbons. With a decrease in temperature, the concentration of wax crystals formed increases, and at a certain threshold level they will precipitate from solution. The oil cloud point is the highest temperature

(1) Reistle, C. E.; Blade, O. C. *A Laboratory Study of Rod Waxes*; U.S. Bureau of Mines Bulletin 348, 1932; pp 125−158.

(2) Escobedo J.; Mansoori, G. A. Heavy Organic Deposition and Plugging of Wells (Analysis of Mexico Experience). *SPE Paper 23696*, 1992.

(3) Carnahan, N. F. Paraffin Deposition in Petroleum Production. *J. Pet. Technol.* **1989** *October*, 1024−1106.

(4) Hansen, A. B.: Larsen, E.; Pedersen, W. B.; Nielsen, A. B. Wax Precipitation from North Sea Crude Oils. 3. Precipitation and Dissolution of Wax Studies by Differential Scanning Calorimetry. *Energy Fuels* **1991**, *5*, 914−923.

(5) Pedersen, K. S.; Skovborg, O.; Rønningsen, H. P. Wax Precipitation from North Sea Crude Oils. 4. Thermodynamic Modeling. *Energy Fuels* **1991**, *5*, 924−932.

(6) Kruka V. R.; Gadena, E.; Long, T. Cloud Point Determination for Crude Oils. *J. Pet. Technol.* **1995**, *8*, 681−687.

(7) Misra, S.; Baruah, S.; Singh, K. Paraffin Problems in Crude Oil Production and Transportation: A Review. *SPE Production & Facilities* **1995**, *February*, 50−54.

(8) Pan, H.; Firoozabadi, A.; Fotland, P. Pressure and Composition Effect on Wax Precipitation: Experimental Data and Model Results. *SPE Paper 36740*, **1996**.

(9) Leontaritis, K. J. The Asphaltene and Wax Deposition Envelopes. *Fuel Sci. Technol. Int.* **1996**, *14*, 13−39.

(10) Dubey, S.; Waxman, M. Asphaltene Adsorption and Desorption from Mineral Surfaces. *Soc. Pet. Eng. Res. Eng.* **1991**, 389−395.

(11) Speight J. G. *The Chemistry and Technology of Petroleum*. M. Dekker: New York, 1991; 760 pp.

(12) Becker, J. R. *Crude Oil Waxes, Emulsions and Asphaltenes*; Penn Well Books: Tulsa, OK, 1997; 276 pp.

(13) Musser, B. J.; Kilpatrick, P. K. Molecular Characterization of Wax Isolated from a Variety of Crude Oils. *Energy Fuels* **1998**, *12*, 715−725.

(14) Hedberg, H. D. Significance of High Wax Oils with Respect to Genesis of Petroleum. *AAPG Bull.* **1968**, *52*, 736−750.

(15) Mozes, G. *Paraffin Products: Properties, Technologies, Applications*; Elsevier: New York, 1982; 335 pp.

(16) Jowett, F. Petroleum Waxes. In *Petroleum Technology*; Hobson, G. D., Ed.; J. Wiley: New York, 1984; pp 1021−1042.

(17) Carlson, R. M.; Moldowan, J. M,; Gallegos, E. J.; Peters, K. E.; Smith, K. S.; Seetoo, W. S. Biological Markers in the C40 to C60 Range: New Marine/Lacustrine Source Indicators. *15th International Meeting on Organic Geochemistry, Oral Communications, Manchester, U.K., September 16−20, 1991*.

(18) Carlson R. M.; Teerman, S. C.; Moldowan, J. M.; Jacobson, S. R.; Chan, E. I.; Dorrough, K. S.; Seetoo, W. C.; Mertani, B. High-Temperature Has Chromatography of High-Wax Oils. In *Proceedings of the Indonesian Petroleum Association, 22nd Annual Convention, October 1993*; pp 483−504.

(19) del Rio, J.-C.; Philp, R. P. High Molecular Weight Hydrocarbons: A New Frontier in Organic Geochemistry. *Trends in Anal. Chem.* **1992a**, *11*, 187−193.

(20) del Rio, J.-C.; Philp, R. P. Oligomerization of Fatty Acids as a Possible Source for High Molecular Weight Hydrocarbons and Sulfur-Containing Compounds in Sediments. *Org. Geochem.* **1992b**, *218*, 869−880.

(21) Philp, R. P.; Bishop, A.; del Rio, J.-C.; Allen, J. Characterization of High Molecular Weight Hydrocarbons (>C40) in Oils and Reservoir Rocks. In *The Geochemistry of Reservoirs*; Cubitt, J. M., England, W. A., Eds.; Geological Society Special Publication **1995**, *86*, 71−85.

(22) Platonov, V.; Proskuryakov, V.; Klyavina, O.; Kolyabina, N. Chemical Composition of Asphaltenes of Crude Oils from Varadero Field in Cuba. *Russ. J. Appl. Chem.* **1994**, *67*, 440−443.

(23) Carbognani, L.; Orea, M.; Fonseca, M. Complex Nature of Separated Solid Phases from Crude Oils. *Energy Fuels* **1999**, *13*, 351−358.

at which formation of wax crystals can be detected.[24−26] Pressure can affect the cloud point of oils in two contrasting ways. First, with increasing pressure, the melting points of pure *n*-alkanes increase, which results in increased cloud points of the oils at higher pressures.[8,9,26] An increase in cloud point of 2 °C/100 bar was suggested as a reasonable estimate for the effect of pressure on cloud point of any dead oils.[26] Second, at higher pressures, the solubility capacity of light hydrocarbon components (methane, ethane, propane) for the wax-forming *n*-alkanes (above C_{20}) increases significantly, and therefore increasing amounts of solution gas in the oil result in a cloud point depression in the order of 10−17°C.[8,9,24,25] Experimental results with live oils have demonstrated that with increasing pressure, the cloud point is initially depressed due to dissolution of light ends in the liquid phase, and at pressures exceeding the bubble point of studied oils, the cloud point starts to increase linearly with pressure.[26]

The wax concentration of an oil influences both the cloud point and rheological behavior of the oil.[4] Data presented in two previous studies[25,27] are compiled in Figure 1 to illustrate that a very small increase (0.05−0.2 wt %) in concentration of HMW (C_{50+}) *n*-alkanes increases oil cloud point with 20−30° C.[28] A much larger increase in concentration of macrocrystalline waxes (20−40 wt %) is required to achieve the same increase in oil cloud point.

Asphaltenes by definition are a solubility class, a petroleum fraction that precipitates in excess of light hydrocarbons. The amount, composition, and molecular weight distribution of asphaltene fractions varies significantly, not only with the origin of the oil, but also with the method of precipitation.[29−32] Asphaltenes are considered as highly condensed polyaromatic structures or molecules, containing heteroatoms (sulfur, nitrogen, and oxygen) and metals (e.g., nickel and vanadium). A predominant view about the state of asphaltenes in oil is that they are colloidally suspended rather than dissolved in the oil. Resins, the lower molecular weight aromatic and polar molecules also containing heteroatoms and metals, which are soluble in oil play an important role in stabilizing the asphaltenes by keeping them in suspension. Asphaltene colloidal structures have been described as micelles with polar asphaltenic

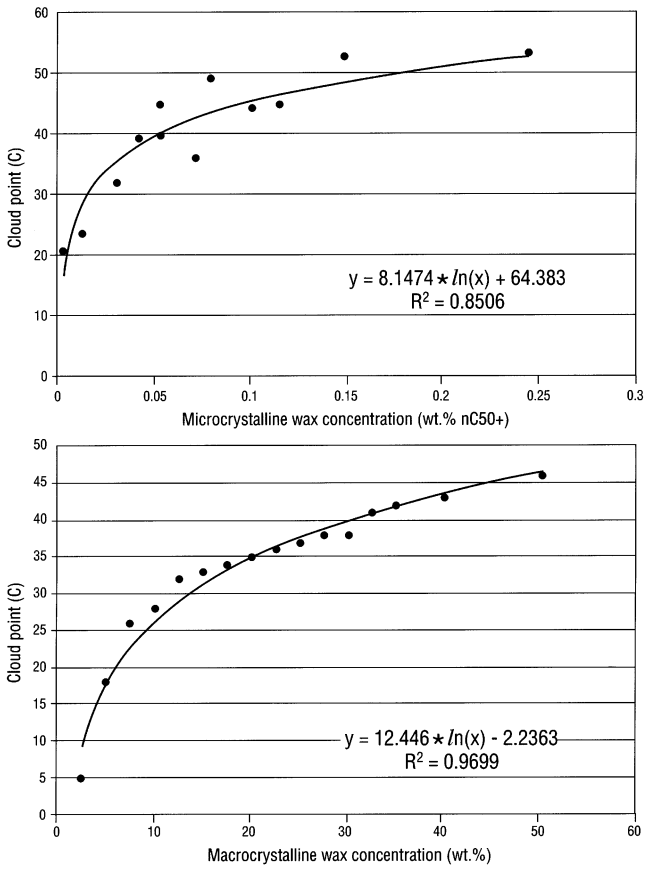

Figure 1. Relationship between cloud point and content of microcrystalline wax (a) and macrocrystalline wax in oils (b). Data from refs 25,27. It should be noted that the methods for cloud point determination were based on the ASTM procedure in ref 27 and as an average of results from four methods (DSC, CPM, FP, FTIR).[25]

interiors surrounded or swollen with resins, with the nonpolar parts oriented toward the oil phase.[33,34] Asphaltene precipitation may occur when the equilibrium of stabilizing forces is disturbed. Changes in pressure, oil composition, and temperature are the main destabilizing factors. Pressure drop has been recognized as especially important in live oils above or close to the saturation point of the reservoir fluid[35,36] and relates to oil compositional changes occurring in the reservoir fluid leading to the onset of asphaltene flocculation. Areas of restricted flow in production equipment (e.g., chokes, collars) associated with pressure differentials are often the location of solid deposit formation. Temperature is usually considered to have an indirect effect on asphaltene precipitation by causing destabilization in the oil composition.[37] Phase transitions (e.g., gas exsolution) and wax precipitation, which is strongly

(24) Rønningsen, H. P.; Bjorndal, B.; Hansen, A. B.; Pedersen, W. B. Wax Precipitation from North Sea Crude Oils. 1. Crystallization and Dissolution Temperatures, and Newtonian and Non-Newtonian Flow Properties. *Energy Fuels* **1991**, *5*, 895−908.

(25) Monger-McClure, T. G.; Tackett, J. E.; Merrill, L. S. Comparisons of Cloud Point Measurements and Paraffin Prediction Methods. *SPE Production & Facilities* **1999**, *14*, 4−16.

(26) Brown, T. S.; Niesen, V. G.; Erickson, D. D. The Effects of Light Ends and High Pressure on Paraffin Formation. *SPE Paper 28505*, **1994**.

(27) Al-Ahmad, M.; Al-Fariss, T.; Obaid-ur-Rehman, S. Solubility Behaviour of a Paraffin Wax in Base Oils. *Fuel* **1993**, *72*, 895−897.

(28) Tchouparova, E. Petroleum Wax Deposition and Production Geochemistry: Experimental Results and Field Examples. Ph.D. Dissertation, University of Oklahoma, Norman, Oklahoma, 1999.

(29) Koots, J. A.; Speight, J. G. Relation of Petroleum Resins to Asphaltenes. *Fuel* **1975**, *54*, 179−184.

(30) Yen, T. F., Chillingarian, G. V., Eds. Asphaltenes and Asphalts. In *Developments Petroleum Sciences Series* 1994, *40A*; Elsevier: Amsterdam, The Netherlands; 459 pp.

(31) Sahimi, M.; Rassamdana, H.; Dabir, B. Asphalt Formation and Precipitation: Experimental Studies and Theoretical Modeling. *SPE J.* **1997**, *June*, 157−169.

(32) Calemma, V.; Rausa, R.; D'Antona, P.; Montanari, L. Characterization of Asphaltenes Molecular Structure. *Energy Fuels* **1998**, *12*, 422−428.

(33) Pfeiffer, J. P.; Saal, R. N. J. Asphaltic Bitumen as a Colloid System. *J. Phys. Chem.* **1940**, *44*, 139−152.

(34) Mitchell, D. L.; Speight, J. F. The Solubility of Asphaltenes in Hydrocarbon Solvents. *Fuel* **1973**, *52*, 149−152.

(35) Hirschberg, A. L.; deJong, N. J.; Schipper, B. A.; Meyers, J. G. Influence of Temperature and Pressure on Asphaltenes Flocculation. *SPE Paper 11202*, **1982**.

(36) de Boer R. B.; Leelooyer, K.; Elgner, M. R. P.; van Bergen, A. R. D. Screening of Crude Oils for Asphalt Precipitation: Theory, Practice and the Selection of Inhibitors. *SPE Paper 24987*, **1992**.

(37) Islam, M. R. Role of Asphaltenes on Oil Recovery and Mathematical Modeling of Asphaltene Properties, In *Asphaltenes and Asphalts*. Yen, T. F., Chillingarian, G. V., Eds.; *Developments in Petroleum Sciences Series*, Elsevier: Amsterdam, The Netherlands; 1994, *40A*, pp 249−298.

sensitive to temperature drops, are two possibilities to be considered.

In addition to pressure, temperature, and oil compositional changes, which are factors controlling both wax and asphaltene precipitation from the reservoir to the surface, several other factors specific to the producing well environment have to be considered, including the flow characteristics and properties of the conduit (e.g., well, pipeline) in which the reservoir fluid is flowing. Changes in all of these parameters result in variations in the amount and composition of formed deposits. Further, shifts in pH invoked by mineral or bacterially produced acids and well stimulations such as acidizing could destabilize the oil−asphaltene equilibrium.[37] Instability due to shear in rod pumps has been identified and is closely related to pressure drops in downhole operations.[38] Neutralization of the electrical charge of colloidal material due to the flow of producing oils is another possible destabilizing factor favorable for solids precipitation.[2] Association of iron sulfide scale, forming directly on the tubing walls and often resulting in corrosion, with organic solid deposition has been identified for wells having sufficient salinity, pressure, and hydrogen sulfide concentration.[39] Recent studies on petroleum solid adherence on well tubing surfaces have distinguished two layers in a naturally formed solid deposit.[40−43] The inner (close to the tubing metal surface) layer is thin (ca. 15 μm) and is characterized as a hard corrosion product containing clay minerals and iron compounds together with linear and cyclic hydrocarbons, aromatic, and carbonyl- and amino-group-containing compounds. The outer layer is thicker (ca. 1 cm) and contains a mixture of petroleum organic compounds and inorganic material such as calcite, dolomite, aragonite, barium sulfate, and sodium chloride. Finally, aging, or the time factor, has to be considered in certain situations of solid deposit formation as well.

Considering the complexity of processes leading to organic solid deposition, the approach of the present study was to take advantage of the nondestruction of the analyzed samples and the capabilities of synchrotron-based microanalyses to investigate a set of organic solid deposits formed in the same well. During the 1996 remediation operations for cleaning the plugged tubing at well Mosteller 1 in Oklahoma, samples of the deposited material were collected from seven strings pulled to the surface in order of increasing depth. The strings are identified according to their location with respect to the surface. The shallowest string is called R1 and the deepest string is called R7. Each string is 45.7 m in length. The uncertainty in the depth location of each sample is estimated at ±22.9 m because marks of the exact sampling depth location were not taken. Depths for the samples are then found to be 22.9, 68.6, 114.3, 160.0, 205.7, 251.4, and 297.1 m. The samples represent a rather unique set, providing control points along the depth profile of solid deposits formed in an actual oil-producing well environment, and cannot be routinely collected because of cost issues. To our knowledge, compositional characterization of such a set of a naturally formed series of solid deposits in the same well has not been undertaken before. The set of samples was initially used to evaluate the changes in *n*-alkane distributions in the deposits by high-temperature gas chromatography (HTGC) and compared with the concurrently ongoing coldfinger experiments on wax deposition.[28, 44] The HTGC results showed a significant shift toward higher molecular weight range *n*-alkane mixtures in deeper deposits (higher temperatures) (Figure 2), consistent with experimental observations and evidencing presence of a temperature differential as expected. A relative increase in the amount of total HMW hydrocarbons (wax) was observed to occur from the deeper (C_{41+} = 201.3 mg/g wax deposit) to shallower (C_{27+} = 214.5 mg/g wax deposit) samples. It should be noted that stated amounts do not refer to the total mass of the solid deposit, which may contain inorganic

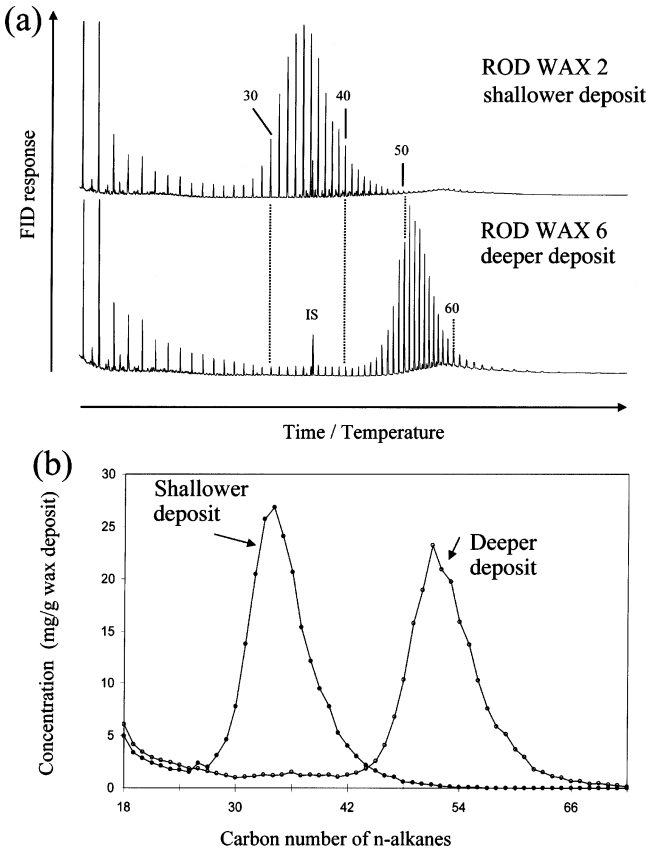

Figure 2. High-temperature gas chromatograms (HTGC) (a) and quantitative results (b) representing the *n*-alkane distributions in two rod wax deposits collected at different depths. A significant shift toward a high molecular weight (HMW) *n*-alkane mixture is observed in the deeper (higher temperature) deposit. IS represents internal standard.

(38) Leontaritis, K. J.; Mansoori, G. A. Asphaltene Flocculation during Oil Production and Processing: A Thermodynamic Colloidal Model. *SPE Paper 16258*, **1987**.

(39) Bittner, S. D.; Zemlak, K. R.; Korotash, B. D. Coiled Tubing Scale of Iron Sulfide − A Case Study of the Kaybob Field in Central Alberta. *SPE Paper 60695*, **2000**.

(40) Cosultchi, A.; Garciafigueroa, E.; Garcia-Borquez, A.; Reguera, E.; Yee-Madeira, H.; Lara, V. H.; Bosch, P. Petroleum Solid Adherence on Tubing Surface. *Fuel* **2001**, *80*, 1963−1968.

(41) Cosultchi, A.; Vargas, J. R.; Zeifert, B. Garciafigueroa, E.; Garcia-Borquez, A.; Lara, V. H.; Bosch, P. AES and EDS Microanalysis of a Petroleum Well Tubing in Cross-Section. *Mater. Lett.* **2002a**, *55*, 312−317.

(42) Cosultchi, A.; Garciafigueroa, E.; Mar, B.; Garcia-Borquez, A.; Lara, V. H.; Bosch, P. Contribution of Organic and Mineral compounds to the Formation of Solid Deposits Inside Petroleum Wells. *Fuel* **2002b**, *81*, 413−421.

(43) Cosultchi, A.; Rossbach, P.; Hernandes-Calderon, I. XPS Analysis of Petroleum Well Tubing Adherence. *Surf. Interface Anal.* **2003**, *35*, 239−245.

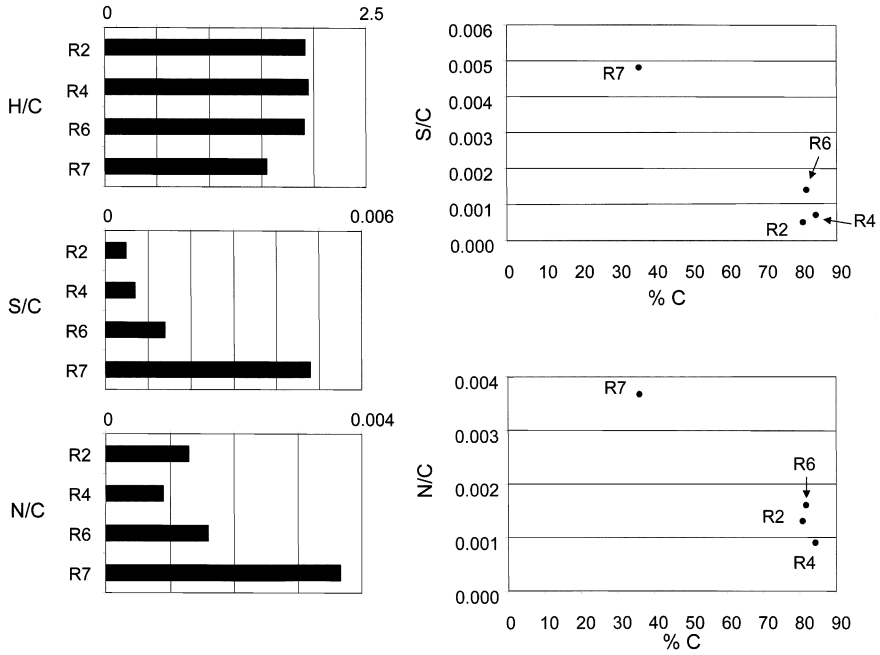

Figure 3. Elemental composition and distribution of H/C, S/C, and N/S atomic ratios in wax deposits formed at increasing depths (temperatures). R2 and R7 are the shallowest and deepest studied deposits, respectively. See text for further description.

components, but only to the mass of organic material soluble in the hot *p*-xylene used in HTGC analyses. The elemental analysis of the deposits revealed significantly lower carbon content, lower H/C and higher S/C, N/C atomic ratios in the deepest available deposit sample (Figure 3).[45] This sample also showed an enrichment in grains of inorganic material up to 500 μm in diameter, while the shallower deposits showed a smaller proportion and size range (up to 100−150 μm) of the inorganic components. These observations taken together suggest that the proportion of organic to inorganic fractions changes significantly in the deepest 100−200 m (depth interval defined by samples RW6 and RW7) of the well strings. These observations as well as the negligible amount of deepest deposits suggest that likely the solid deposition started first in the producing strings rather than in the producing reservoir interval where it could have caused additional formation damage.

The purpose of the present study is to extend the compositional characterization of the above-described set of naturally formed petroleum deposits at a microanalytical level by using synchrotron radiation-based techniques. A major advantage of these techniques is that they are nondestructive and do not require a preliminary treatment (e.g., dissolution, fractionation, centrifugation, etc.), as do many of the traditional methods, while providing a level of investigation at the 10 μm × 10 μm scale. The present study utilizes the advantages of two main synchrotron radiation-based techniques: X-ray fluorescence (XRF) and Fourier transform infrared (FTIR) spectroscopy. Results from synchrotron K-edge sulfur X-ray absorption near-edge structure (XANES) for the same series of samples are used for comparison. Results from the initial phase of this study have been reported.[44−46] The study attempts to further clarify the macroscopic phenomena defined by the sample set as described above and evaluate the applicability of the techniques to studying solid-semi-solid complex petroleum mixtures in the context of organic solid deposition and wax and asphaltene aggregation and precipitation. Specific questions that the study addresses are: What are the distribution and interactions between organic and inorganic components in the series of solid petroleum deposits formed along the depth profile in the same producing well? Is the organic and inorganic distribution heterogeneous within the same sample and along the depth profile defined by the samples? What is the scale of heterogeneity?

Advantages Of Synchrotron Radiation-Based Microanalysis. Elemental analysis using emission of characteristic X-rays is a well-established scientific method. The success of this analytical method is highly dependent on the properties of the source used to produce the X-rays. X-ray tubes have long existed as a principal excitation source, but the development of the synchrotron radiation X-ray source that has taken place during the past 40 years has had a major impact on the general field of X-ray analysis.[47−49] Notable properties of the synchrotron X-ray source include the continuous

(44) Chouparova, E.; Philp, R. P.; Nagarajan, N. R.; Whitson, C. *n*-Alkane Distributions in Organic Solid Deposits vs Temperature of Deposition. *J. Am. Chem. Soc.* **2000**, *S219*, 103-GEOC.

(45) Chouparova, E.; Vairavamurthy, A.; Whitson, C.; Philp, R. P. Sulfur Speciation in Rod Wax Deposits from an Oil Producing Well, Eastern Anadarko Basin, Oklahoma: A Sulfur K-edge XANES Spectroscopy Study. BNL-68061, November 2001.

(46) Chouparova, E.; Feng, H.; Lanzirotti, A.; Jones, K. Trace Metal Distributions in Rod Wax Deposits Formed in an Oil-Producing Well, Anadarko Basin, Oklahoma (abstract). Presented at *Seventh Annual International Petroleum Environmental Conference, Albuquerque, New Mexico, November 7−10, 2000*.

(47) Jones, K. W. Synchrotron Radiation-Induced X-ray Emission (SRIXE). In *Handbook of X-ray Spectrometry*, 2nd ed., *revised*; Van Grieken, R., Markowicz, A., Eds.; Marcel Dekker: New York, 2002; Chapter 8, pp 500−558.

(48) Jones, K. W. Applications in the Geological Sciences. In *Microscopic X-ray Fluorescence Analysis*; Janssens, K., Rindby, A., Adams, F., Eds.; John Wiley & Sons Ltd.: Sussex, England, 2000; Chapter 8, pp 247−290.

(49) Jones, K. W.; Feng, H. Microanalysis of Materials Using Synchrotron Radiation. In *Chemical Applications of Synchrotron Radiation, Volume 12B*, T. K. Sham, Ed.; World Scientific Publishing Company: Singapore, 2002; Chapter 22, pp 1010−1054.

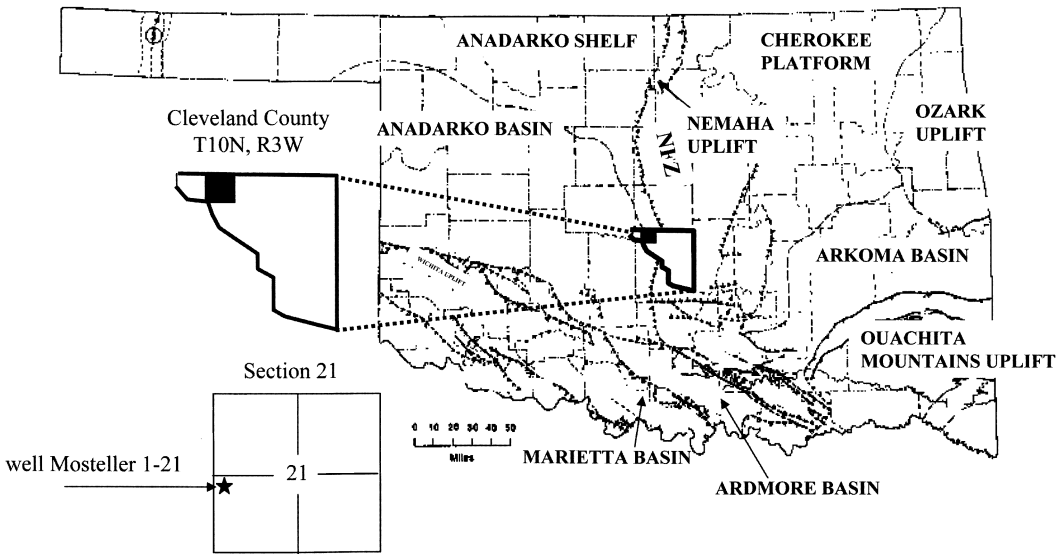

Figure 4. Map of Oklahoma showing the location of the Mosteller 1-21 well.

range of energy (from infrared to hard X-rays) that allow monoenergetic beams to be produced over a wide range of energies, high degree of photon polarization, and photon fluxes many orders of magnitude higher than from X-ray tubes; this has made possible major advances in the possible chemical applications. The high photon flux that is delivered to the sample ensures a reduced time for a given experiment, improves the spatial resolution, and reduces the elemental detection limits.

Facilities at the National Synchrotron Light Source (NSLS) were used for the present experiment. The X-ray beams are produced as the electrons in the storage rings pass through the bending magnets used to contain the circulating beam or through undulator or wiggler insertion devices, which can be used to increase the beam intensity or shift the energy to higher values. Radiation in the infrared and vacuum ultraviolet regions is produced by the NSLS low-energy storage ring and in the X-ray region by the high-energy storage ring.

The electron energy in the high-energy storage ring is high enough to produce X-rays over an energy range sufficient to produce K-X-rays from elements to about $Z = 40$ with good efficiency and L-X-rays throughout the periodic table. This is highly suitable for X-ray microscopy-based synchrotron radiation-induced X-ray emission (SRIXE), and, in particular, X-ray fluorescence (XRF). The lifetime of the stored beams is many hours, so that in practice, work with the synchrotron source is similar to work with a standard X-ray tube.

In comparison to conventional X-ray fluorescence and microbeam analyses, synchrotron XRF spectroscopy has several major advantages: a low elemental detection limit (around 1 part-per-million); X-ray beams that can be focused down to a 1-to-10 μm spot size on the sample; ability to analyze samples in-situ; and nondestructive and rapid analysis. Similarly, FTIR spectroscopy measurements are facilitated because the brightness of the synchrotron source is 100−1000 times that of thermal sources so that the IR beam can be focused to a narrow spot close to the diffraction limit of 5 μm at 2000 cm^{-1}. Furthermore, the advantage of the broadband synchrotron source over other strong sources (e.g., single-wavelength infrared lasers) is the ability to collect full infrared spectra in a short time period at high signal-to-noise ratio.

Experimental Section

Samples. Well Mosteller 1 is located in Cleveland County, OK (T10N, R2W, section 21). Geologically, it is situated at the easternmost part of Anadarko Basin, approximately 20 miles west of the Nemaha Fault Zone (Figure 4). The samples studied represent a series of semisolid to solid petroleum deposits formed at different depths in the production strings (sucker pump rods) from the Mosteller 1 well during oil production from the Viola carbonate reservoir of Ordovician age. The deposit material sampled was collected and preserved in small (1 in. × 0.5 in.) tightly closed containers. Initial gas−oil ratio and gravity of the oil were 1880 scf/bbl and 40.1 API, respectively. Total depth of the well is 2916 feet, with a maximum-recorded temperature of 138 °F (59 °C).

The deposits represent dark brown to black solids to semisolids. Preliminary visual inspection of thin spreads of material under reflected light with a binocular microscope showed that the deepest deposit is enriched in grains up to 500 μm in diameter covered with organic material. After treatment with carbon tetrachloride and toluene, some of the organic material was dissolved and the cleaned parts of the grains were found to resemble carbonate particles. The shallower deposits showed a much smaller proportion and size range (up to 100−150 μm) for this type of inorganic material. This could result from a gravitational fractionation of the particles.

The samples for XRF analysis were prepared by pressing them to a uniform thickness of 1 mm. They were mounted between two 0.00725-mm polyimide films for the exposure to the X-ray beam. The deepest sample (RW7) showed some irregularities in thickness (2−3 mm), which could be attributed to the small amount of deposit and presence of the relatively large inorganic grains that appeared on the visual inspection with the binocular microscope. FTIR analysis was performed only on the deepest wax deposit (RW7). The sample was prepared by pressing a small amount of material on the IR slide to achieve a thin and relatively uniform thickness distribution.

Synchrotron X-ray Fluorescence Microspectroscopy. The XRF experiments were performed at the NSLS beam line X26A. The experimental set up (Figure 5a) consists of the following: (1) a monochromator, collimator, and focusing lenses for producing a microbeam; (2) a computer-controlled sample stage for point-by-point mapping of the elemental

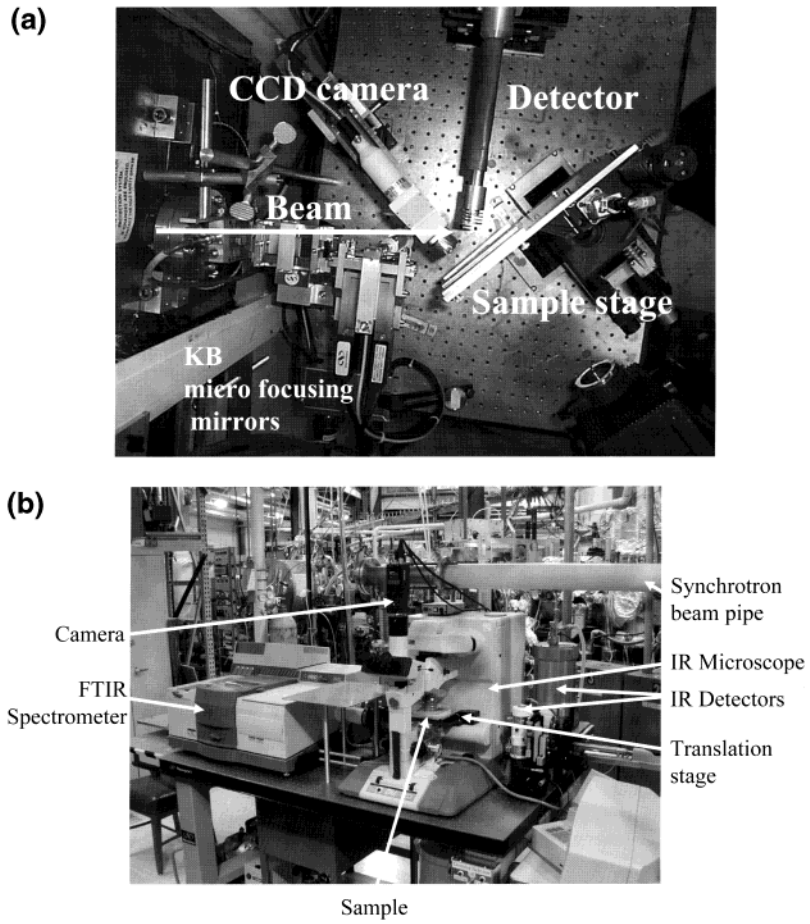

Figure 5. (a) Photograph of the X26A beam line X-ray microprobe experimental apparatus. (b) Photograph of the U2B micro FTIR beam line.

spatial distributions; (3) an X-ray detection system consisting of a 30 mm^2 lithium-drifted silicon X-ray detector with an energy resolution of approximately 160 eV for detection of fluorescent X-rays; and (4) a charged-coupled device (CCD) camera to aid in positioning the X-ray beam on the sample. The source distance for the X-ray microprobe located on the NSLS X26A beam line is 9 m. The experiments were performed using a monoenergetic beam (16.7 keV) collimated to 150 μm $\times$ 350 μm size and then focused, with Kirkpatrick Baez (KB) micro-focusing mirrors, to a 10 μm $\times$ 10 μm size with a concomitant increase in the photon flux. The energy range for the fluorescent X-rays was from 4 to 16.7 keV with an acquisition time of 15 min for point spectra analysis. According to Jones,[48] trace element detection limits are around 10 femtograms (fg) for elements around Fe, Cu, and Zn using K-X-ray detection and similar values for elements around Pb using L-X-ray detection were obtained with a similar system in the past. Detection limits for the present apparatus with improved focusing and smaller source distance are below 1 fg.

Data on individual spots and regions-of-interest line scans were obtained by analysis of the fluorescent X-ray energy spectra. The semiquantitative analysis consisted of first fitting the peaks' background in the X-ray spectra in order to obtain the elements peak areas. Then the peak areas were normalized to the ion chamber and the live time, thus accounting for variations in the ring current and in density/concentration among different spots in the sample(s), respectively. Normalized peak areas (expressed in counts per minute), which are proportional to the concentration, for each element were used to construct depth profiles of the metal distributions in the studied series of wax deposits. Errors due to possible matrix and thickness variations among particular microanalytical points in the sample(s) were evaluated using a modified version of the public-domain NRLXRF program.[50] The program takes into account the absorption of the incident beam by air and the beryllium windows that isolate the beam line vacuum from the ring vacuum; photo-ionization efficiencies; fluorescence yields, self-absorption; secondary fluorescence; and fluorescence beam absorption by air and detector filters, including the polyimide tape on the samples. Test calculations using varying sample thickness and densities from 1000 μm to 3000 μm and from 0.85 to 8 g/cm^3 (wax, sedimentary rock, corrosion particle), respectively, were performed to evaluate their possible effects on estimated peak areas. The results showed that neither thickness nor density variations in these ranges could account completely for the significantly higher metal abundances observed in the deepest deposits, as discussed later, suggesting that the observations are mainly due to compositional differences.

Synchrotron FTIR Apparatus. An infrared beam from the NSLS UV ring imaged through a commercial FTIR spectrometer (Nicolet Magna 860) was focused onto a sample using an infrared microscope (Nicolet NicPlan), Figure 5b. Samples were placed onto IR-reflective slides (Low-e Microscope slides, Kevley Technologies, Chesterland, OH). IR light irradiates a sample point of 10 μm $\times$ 10 μm, reflects from the IR-reflective slide, and passes again through the sample point before it reaches a narrow-band HgCdTe (MCT) detector. The slides are partially transparent in the visible range so that positioning of the samples under the IR microscope is simple.

(50) Birks, L. S.; Gilfrich, J. V.; Criss, J. W. NRLXRF, A Fortran IV Program for X-ray Fluorescence Analysis: User's Guide, *NRL Report 8077*. Naval Research Laboratory: Washington, DC, 1977; Criss J. W.; Birks, L. S.; Gilfrich, J. V. Versatile X-ray Analysis Program Combining Fundamental Parameters and Empirical Coefficients. *Anal. Chem.* **1978**, *50*, 33.

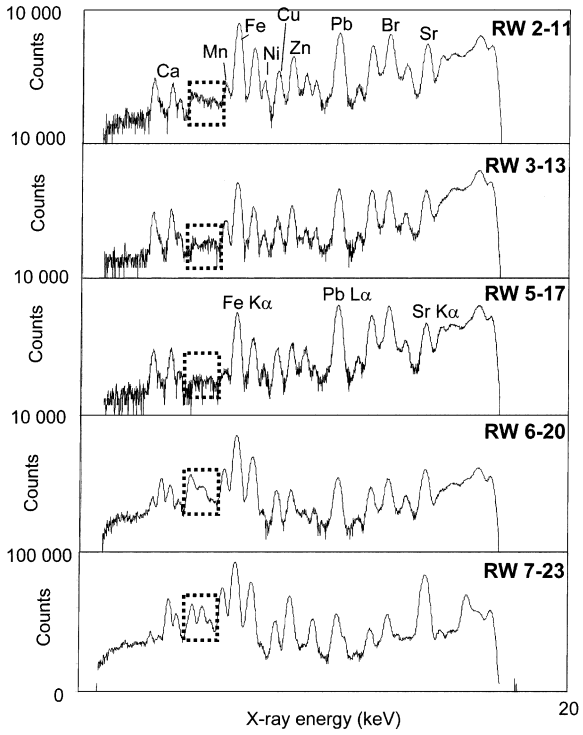

Figure 6. XRF spectra taken on deposits formed at increasing depths/temperatures (from RW2 to RW7) in the same oil-producing well. Note the increased abundance of several peaks in the energy range 4.465 to 5.947 keV (dashed square) only in the deepest two samples (RW6 and RW7). The peaks correspond to the energy positions of Ba, Ti, V, and Cr.

The visible picture of the sample area from which the measurement is taken is observed using a SONY XC-711 CCD camera and stored as a bitmap image. Both single-point spectra and infrared mapping were used in the course of experiments by collecting 128 scans at 4 cm^{-1} resolution in the mid-IR range (4000−600 cm^{-1}). For quantitative purposes, the samples for the IR reflection measurements should have a uniform thickness of the order of 10 μm, so that the absorbance is directly proportional to the sample concentration. However, since the absorption probability (and hence the concentration of organic material) varies with the grain composition and/or structure, no direct proportionality is possible among grains. The data analysis is therefore limited to qualitative comparison of the IR spectra, for which no special processing is necessary.

Results and Discussion

XRF Spectroscopy Results. Selected standard energy dispersive spectra of analyzed samples are presented in Figure 6 where the *y*-axis is logarithmic counts and the *x*-axis is the X-ray energy from 0 to 16.7 keV. A comparison of the point spectra in Figure 6 demonstrates that Ca, Fe, Ni, Cu, Pb, and Br peaks are common in all samples. Increased abundances of several peaks in the energy range 4.465 to 5.947 keV appear only in the spectra of deepest two deposits (dashed square region in Figure 6). These peaks correspond to the energy positions of Ba, Ti, V, and Cr. Determination of which of these elements is present in a particular spectrum was based on the combination of components resulting in the best fit with the experimental spectrum.

Depth profiles constructed using normalized peak areas demonstrate the relative elemental abundances in the deposits formed at different depths along the studied well (Figure 7). The relative abundances are expressed as normalized counts per minute and are proportional to the element's concentration in the sample volume of analysis. The first observation derived from the presented results is that the deepest two deposits (RW6 and RW7) are markedly different from the shallower deposits. They are characterized with five to twenty times higher abundances of Fe, Ca, Sr, V, Ti, Cr, and Ba, depletion of Br, and no detectable abundances of Ir. The anomalously high abundances of the above elements may be related to a higher proportion of inorganic material in the deepest two deposits and a possible contribution from corrosion, reservoir carbonate and barite (drilling mud) particles. Iron, calcium, and barium have been reported in solid deposits recovered from well tubings.[40,51] A selective enrichment with Ni, Zn, and Pb is observed at one of the analytical points (24) of the deepest deposit RW7. Vanadium, titanium, and chromium are detected only in the deepest two deposits (RW6 and RW7) and at point 12 of the shallower deposit RW2. The latter has unusually high abundances of Ca, Mn, Ni, and Cu for a shallow deposit. The depth profile results also suggest a significant variability in Sr, Mn, V, Ti, Cr, Ba, and Zn abundances among different spots of the same sample (especially in the deepest two deposits RW6 and RW7). To further investigate the heterogeneity in the metals distribution in the same deposit, particularly the scale of heterogeneity, the results from an XRF line scan on a region of interest in deposit RW5 are presented in Figure 8. The line scan encompasses a total distance of 1.4 mm and the point spectra are taken with a step size of 100 μm. A reflected light micrograph showing the position of the line scan in the sample is presented in Figure 9. The results demonstrate heterogeneity in the metals distribution on a scale of several hundred micrometers within the same sample (Figure 8). A preferential enrichment with different metals is observed at the following: point 4—Sr, Ca, Zn, Ni, as well as Fe, Mn, Ti, V, and Si; point 9—Fe, Mn, Ti, V, Si, as well as Sr; points 10 and 11—Cu and Pb; point 8—Pb. The increased abundance of both Ca and Sr at point 4 suggests the presence of a carbonate particle. In addition, the micro-photographic image suggests the presence of several isolated grains, possibly representing inorganic material, in the analytical area of point 4. On the other hand, the high abundance of Fe in addition to Si and Ti at point 9 is suggestive of the presence of a clay particle (silicates) and/or a metal particle (e.g., a corrosion product from the well). Iron species reportedly enhance organic retention, and Fe_2O_3 has been identified to be an especially active promoter of polar organic compound retention on clays.[23] An enrichment of both Cu and Pb is detected at points 10 and 11.

Knowing that the petroleum deposits studied represent a mixture of organic and inorganic constituents, the metal distributions (described above) and concentrations will be influenced by the metal content in both organic and inorganic phases. The metallic constituents in petroleum are known to exist in two major groups—metalloporphyrins and non-porphyrin metal chelates. Upon fractionation of petroleum, the metallic constitu-

(51) Kotlyar, L. S.; Sparks, B. D.; Kodama, H.; Grattan-Bellew, P. E. Isolation and Characterization of Organic-Rich Solids Present in Utah Oil Sand. *Energy Fuels* **1988**, *2*, 589−593.

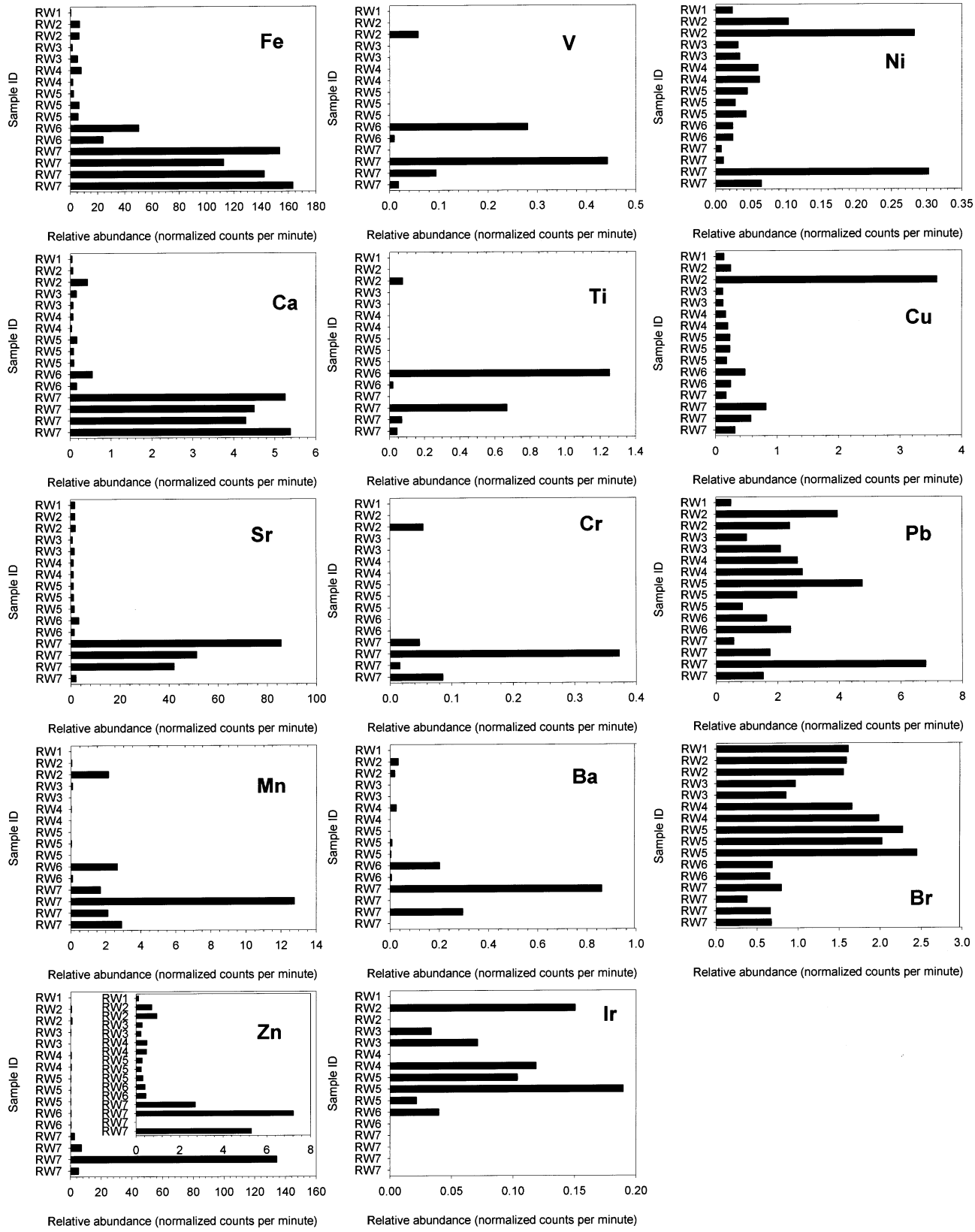

Figure 7. Deposit depth profiles demonstrate relative elemental abundances in the studied series of solid petroleum deposits by XRF spectroscopy. Note that the abundances of Sr, Ca, and Fe were orders of magnitude higher in the deepest two deposits where the total amount of deposit and organic material are much smaller. These metals are shown to be most likely associated with carbonate particles in the deposits, which are found to form the polar Type II of aggregates (see Figure 10).

ents are often observed to concentrate in the asphaltene fraction.[10,52,53] Nickel- and vanadium-containing compounds are the two best-characterized and -studied metallic constituents in the oils. Vanadium, titanium, and chromium occur in detectable abundances only in the deepest two deposits (Figure 7). The proportion of inorganic-to-organic material increases in the deepest deposits based on the elemental analysis results (Figure

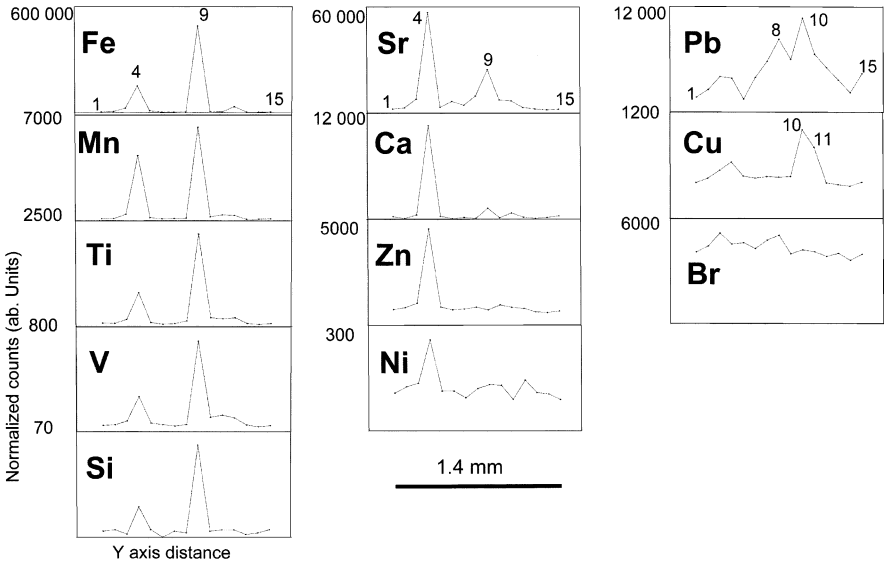

Figure 8. Variability of heavy elements observed in a 1-dimensional scan by XRF spectroscopy. Total distance of the line scan is 1.4 mm, and point spectra are taken with a step size of 100 μm.

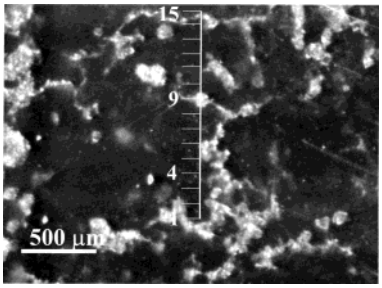

Figure 9. Optical image (reflected light) of deposit sample RW5 showing the position of the XRF line scan.

3), and corresponds to the occurrence of these metals. On the other hand, preferential enrichment of vanadium in the organic phase could occur under strongly reducing, H_2S-rich environments.[53] The possibility of hot H_2S-enriched gas migration in the studied well region of Anadarko Basin could find some support in several geological considerations, as discussed elsewhere.[54] Another source of the hydrogen sulfide down hole could be related to possible microbial activity that could have been initiated or introduced by drilling mud or chemicals added to the well. A clear-cut discrimination of vanadium association with the inorganic or organic phase in the deepest deposits is not reliable at this stage. In contrast to vanadium, nickel is detected along the depth profile of all deposits (Figure 7). Temperature-induced solubility differences and variations in Eh−pH conditions[52,53] of the macro- and micro-chemical environment in the producing tubing during deposit formation could all be factors contributing to the observed metal distributions in the organic phase of the deposits. Abundances of Sr and Ca in the deepest deposit samples were orders of magnitude higher than those in samples taken at the shallowest depths. This was attributed to an increased abundance of carbonate particles, originating from the producing carbonate reservoir, and a low proportion of the organic phase. A possible source of the similarly high Fe abundance in the same deposit could be corrosion from the tubing itself (see discussions below) or from an old iron bridge plug in the well below the producing Viola reservoir.

Synchrotron FTIR Results. The XRF results presented above show metal distributions in the deepest deposits attributed to a relative predominance of inorganic carbonate and/or clay particles. To obtain additional compositional information about the organic material of the deposit and its association with the inorganics, synchrotron FTIR analyses were performed on the deepest deposit RW7. Photographs and typical IR spectra on different aggregates observed within the sample are presented in Figures 10 and 11, respectively. The data demonstrate two distinct types of IR spectra for the studied aggregates: predominantly nonpolar (Type I) and predominantly polar (Type II). Mixed spectra, intermediate between Type I and II spectra, are also observed in some of the aggregates (RW7-27, RW7-28).

Type I spectra are relatively simple and characterized by strong absorption bands of C−H symmetrical and asymmetrical stretching and bending vibrations in CH_2 and CH_3 groups in the regions 2962−2853 cm^{-1} and 1465−1375 cm^{-1}, respectively. The absorption band near 1375 cm^{-1} (δ_s of methyl C−H bonds) is very stable in position, indicating that the methyl group is attached to another carbon atom.[55] In addition, the spectra of this type of aggregates have two absorption bands at 730 and 720 cm^{-1}. The $-(CH_2)_n-$ *n*-phase rocking vibration for long straight chain methylene chains in the liquid state commonly appears at 726−720 cm^{-1}, and it is known that in the solid state, it splits into a doublet at 730 and 720 cm^{-1},[55] as observed in Type I spectra. These absorption characteristics can be related to a predominance of long-chain normal and isoalkanes, which were

(52) Lewan, M. D.; Maynard, J. B. Factors Controlling Enrichment of Vanadium and Nickel in the Bitumen of Organic Sedimentary Rocks. *Geochim. Cosmochim. Acta* **1982**, *46*, 2547−2560.

(53) Lewan, M. D. Factors Controlling the Proportionality of Vanadium to Nickel in Crude Oils. *Geochim. Cosmochim. Acta* **1984**, *48*, 2231−2238.

(54) Chouparova, E.; Rottmann, K.; Philp, R. P. Geochemical Study of Oils Produced from Four Pennsylvanian Reservoirs in Prairie Gem Field, Central Oklahoma. In *Pennsylvanian and Permian Geology and Petroleum in the Southern Midcontinent, 1998 Symposium;* K. S. Johnson, Ed.; Oklahoma Geological Survey Circular 104, 2001, pp 105−113.

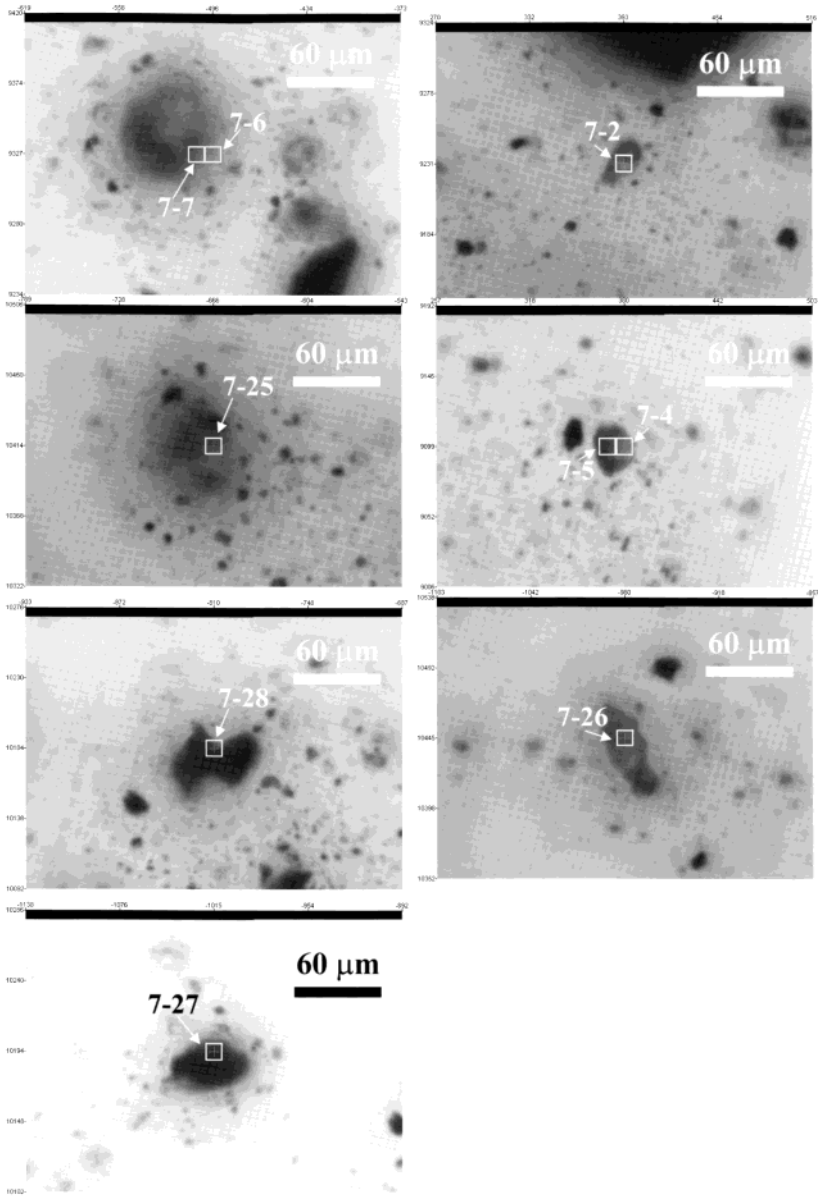

Figure 10. Optical images of different aggregates observed in the deepest deposit sample RW7. The regions where IR spectra are obtained are indicated with squares.

independently identified by previous high-temperature gas chromatography studies of these samples (Figure 2). Medium absorption around 1600 cm^{-1} in the spectra could be related to −C═C− stretch in aromatic structures. Small but distinctive absorptions in the 2800−2550 cm^{-1} region, indicative for −SH stretching, suggest the possible presence of aliphatic thiols. FTIR mapping further reveals the hydrocarbon distribution in a single aggregate of this type (Figure 12). The spectra shown for point spectra 7-6 and 7-7 in Figure 11 represent typical spectra for the whole aggregate. A map of the characteristic CH_2 and CH_3 absorption bands in the 2962−2853 cm^{-1} and 1465−1375 cm^{-1} region are presented in Figure 12, parts a and b, respectively. The absorption bands of the characteristic for the carbonyl group region of 1725−1695 cm^{-1} in this aggregate signify the presence of carboxylic acids, most likely long-chain acids. They appear to be distributed irregularly toward the periphery of the aggregate (Figure 12c). The occurrence and distribution of carboxylic acids could be related to the processes associated with oil−water−mineral interfacial phenomena and interactions in microemulsions.[56] A photomicrograph of the sample and position of the measurements is shown in Figure 12d.

Type II infrared spectra and aggregates demonstrate a more complex fingerprint compared to Type I spectra (Figure 11). Type II spectra show the characteristic bands of CH_2 and CH_3 groups but with relatively lower intensity compared to Type I spectra and aggregates. In addition, bands indicative of aromatic, sulfur-, and nitrogen-containing compounds are present together with a well-defined hydrogen-bonding region that could be associated with NH and/or OH groups. The spectra show absorption bands indicative of para-substituted aromatics (860−800 cm^{-1}, 1600 cm^{-1}, overtone absorp-

(55) Lin-Vien, Daimay; Fateley, William; Colthup, Norman B.; Grasselli, Jeannette G. *Handbook of Infrared and Raman Characteristic Frequencies of Organic Molecules*; Academic Press: Boston, MA, 1991.

(56) Sjöblom ,J.; Lindberg, R.; Friberg, S. E. Microemulsions − Phase Equilibria Calculations, Structure, Applications and Chemical Reactions. *Adv. Colloid Interface Sci.* **1996**, *95*, 125−287.

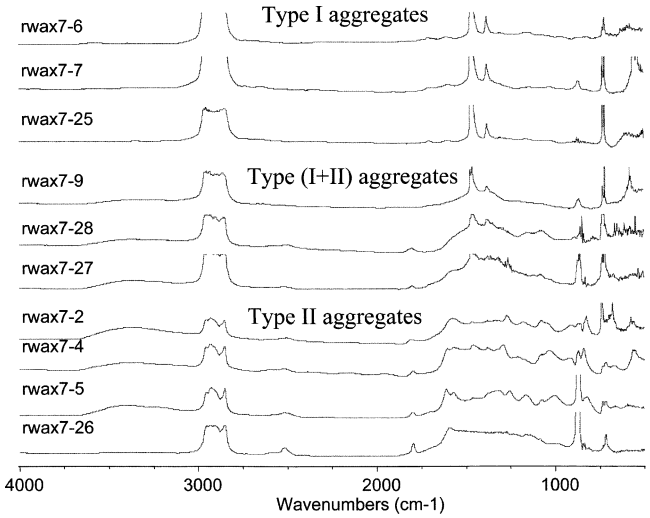

Figure 11. Examples of typical FTIR spectra for Type I, Type (I + II), and Type II aggregates.

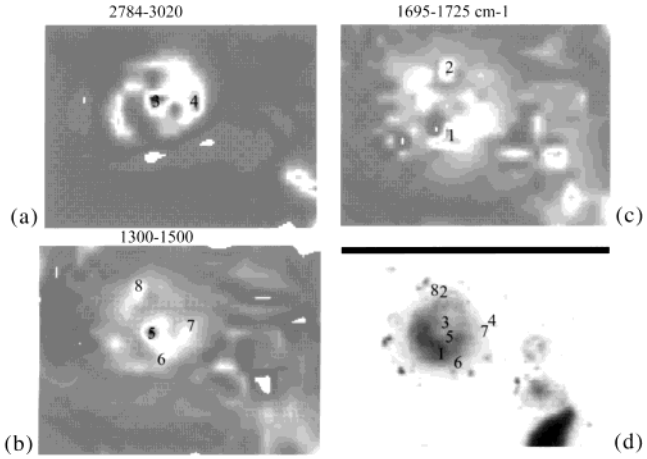

Figure 12. FTIR mapping of a single Type I aggregate in the deepest deposit RW7. Maps representing the distribution of characteristic CH_2 and CH_3 absorption bands (2962−2853 cm^{-1}, 1465−1375 cm^{-1}) in the aggregate (a, b) and carbonyl group bands (1725−1695 cm^{-1}) in the same aggregate (c). The numbers on the micro-photograph (d) can be used as reference points for the aggregate position on the infrared maps.

tions in the region 2000−1700 cm^{-1}), sulfoxides (S═O stretching absorption in 1055−1000 cm^{-1}), sulfonic acids (two strong absorptions in the 1200−900 cm^{-1} region, and a broad absorption in 3400−3200 cm^{-1} that could be assigned to −S−OH stretching), and/or sulfonic acid salts (RW7-2 only, characteristic absorption of $-SO_3$ structure at 1175 cm^{-1}, and pronounced absorption in the 3400−3200 cm^{-1} region that may be assignable to water molecules associated with the salts). Structures containing −S−O−R (R aliphatic) and $-SO_2-$ are indicated by absorptions in 1000−770 cm^{-1} and two absorptions between 1335 and 1175 cm^{-1}. Absorptions in 770−665 cm^{-1} and 1000−910 cm^{-1} point to S−O−C structures. These observations are in agreement with the results from a K-edge XANES spectroscopy study on the same set of deposit samples.[45] The presence of various oxidation state sulfur species (di/polysulfides or elemental sulfur, thiophenic/sulfidic, sulfoxide, sulfone, sulfonic acids, and sulfate) in the deposits and a distinct shift in relative abundance of oxidized to reduced forms with increasing sampling depth of the deposits are evident (Figure 13).[45] The presence of sulfonic acids is indicated by both FTIR and K-edge XANES spectroscopy results. Studies on the asphaltene inhibitor representing dodecyl benzene sulfonic acid have shown that for oils with high content of basic functionalities this inhibitor, when introduced at low concentrations, can increase organic solid precipitation rather than inhibit it.[57−60] Introduction of such an inhibitor at low amounts is possible for well Mosteller 1, but cannot be constrained with documented information. Further on, it was found that characteristic bands for a number of inorganic compounds are specifically associated with Type II aggregates, mainly carbonates of Ca, Fe, Mn, Ni, Zn, and Pb. Figure 14 demonstrates a comparison of Types I and II spectra and aggregates with the IR spectrum of a standard calcium carbonate. This observation provides an independent line of evidence about the likely chemical state of at least part of the trace metals in the deepest deposits and complements the XRF results demonstrating increased concentrations of both Sr and Ca at different points within a sample and specifically in the deepest petroleum deposit sample. In addition, it provides evidence for the organic−inorganic phase distributions and associations. Characteristic absorption bands for silicon-containing groups are apparent only in Type II spectra and aggregates. Thus, the strong absorption in the 1110−1000 cm^{-1} region could be related to stretching vibrations of Si−O attached to aliphatic hydrocarbon groups, even though this region overlaps with the sulfoxides absorption bands in 1080−1070 cm^{-1}. The absorption bands in 910−830 cm^{-1} could be indicative of Si−O stretching vibrations in Si−OH and/or Si−H attached to a radical (950−800 cm^{-1}) and are apparent only in Type II spectra.

Discussion

Aggregates from the deepest deposit are found to be of several distinct types. Predominantly nonpolar (Type I) aggregates contain long chain alkanes, aromatic compounds, and aliphatic thiols, consistent with characteristics of "wax" type aggregates. The presence of carboxylic acids distributed irregularly toward the periphery of a FTIR-mapped aggregate of this type was indicated. Predominantly polar (Type II) aggregates consist of aromatic structures, sulfur-, nitrogen-, and oxygen-containing compounds, some aliphatic structures, and water molecules possibly associated with salts. The characteristics of these types of aggregates are consistent with "asphaltene" type aggregates. These types of aggregates are found associated with inorganic carbonate particles. This association is consistent with previously reported selectivity of carbonate rocks to oxygenated compounds.[61] There are also indications suggesting clay−organic complexes formation and pro-

(57) Chang, C.-L.; Fogler, H. S. Stabilization of Asphaltenes in Aliphatic Solvents Using Alkylbenzene-Derived Amphiphiles. 2. Study of the Asphaltene−Amphiphile Interactions and Structures Using Fourier Transform Infrared Spectroscopy and Small-Angle X-ray Scattering Techniques. *Langmuir* **1994**, *10*, 1758−1766.

(58) Rogel, E.; Leon, O.; Espidel, J.; Gonzalez, J. Asphaltene Stability in Crude Oil. *SPE Paper 53998*, **1999**.

(59) Rogel, E.; Leon, O.; Espidel, J.; Gonzalez, J. Asphaltene Stability in Crude Oil. *SPE Production & Facilities* **2001**, *May*, 84−88.

(60) Rietjens, M.; Nieuwpoort, M. Acid-Sludge: How Small Particles Can Make a Big Impact. *SPE Paper 54727*, **1999**.

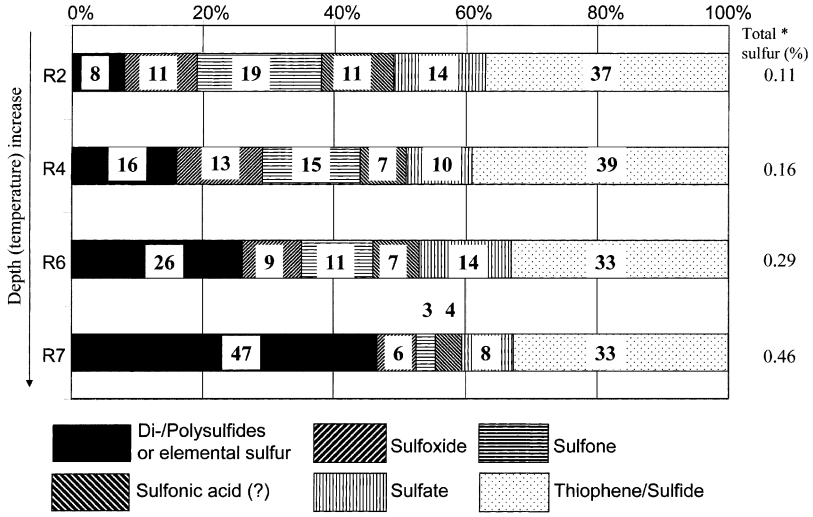

Figure 13. Estimated relative proportions of different sulfur functionalities by K-edge XANES spectroscopy in studied rod wax deposits (R2, R4, R6, R7). Total sulfur content (wt % of deposit) was obtained from elemental analysis.

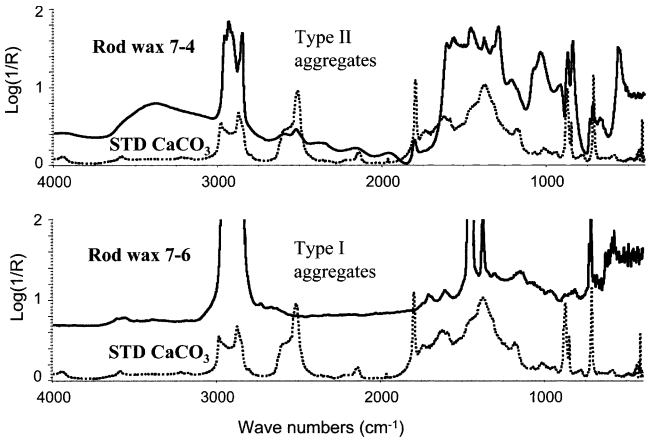

Figure 14. FTIR spectra comparison of $CaCO_3$ standard with typical Type I and Type II aggregates in the deposit.

cesses associated with microemulsion−inorganic solid interactions,[56,62] which can be expected considering the surface active characteristics of asphaltenes, resins, organic acids, metallic salts, scales, and clays (indicated in the composition of Type II polar aggregates). Overall, the results indicate that the polar type aggregates are the result of both ionic interactions and surface precipitation.[63,64] Aggregates with mixed between Type I and II spectra are also observed. The presence of mixed polar/nonpolar aggregates can be related to previous observations regarding the possibility of adsorption of resins and asphaltenes with the HMW hydrocarbons resulting in their coprecipitation.[12,13,23] The size of aggregates observed in the deepest deposit are in the order of 10−60 μm. Since the largest asphaltene micelles reportedly can be considered in the order of 2 μm,[65] it is clear that observed aggregates in the deepest deposit are the result of an aggregation process, most likely diffusion-limited cluster−cluster aggregation.[31] Wax deposition is also a result of aggregation phenomena in the oil solution. Carboxylic acids can join pure wax clusters with their nonpolar ends. It can be speculated that the presence of carboxylic acids observed toward the periphery of the mapped nonpolar aggregate reflects such a process of cluster−cluster aggregation. Particles and clusters of different types could stick together upon collision in the oil solution under appropriate conditions, further aggregate, and ultimately become a part of the deposit. This could be a process leading to formation of the observed mixed polar/nonpolar aggregates; and carboxylic acids may be playing an important role there.

The depth profile of solid deposits formed in the studied single well can be characterized with the following main trends from deeper to shallower samples: (1) amount of deposits increases, a complete tubing plugging occurs at shallower levels; (2) concentrations of inorganic components decrease; (3) sulfur-containing compounds in the deposits shift relative abundances from predominantly reduced to predominantly oxidized forms; (4) carbon content and H/C atomic ratio increase, S/C and N/C atomic ratios decrease; (5) HMW *n*-alkane mixtures (wax components) shift the maximum of their distribution from higher to lower molecular weight mixtures; (6) some metals (V, Ba, Ti, and Cr) are detectable only in the deepest samples; (7) elements present in all samples along the depth profile are Ca, Fe, Ni, Cu, Pb, and Br.

The shift in carbon number distribution of HMW *n*-alkane mixtures signifies a temperature change along the producing well tubing as expected. Even though a relative increase in amount of HMW mixtures is observed at shallower depths, the amount of wax components along the depth profile of the deposits is below ca. 20%. The remainder should be attributed to asphaltenes, inorganic particles, trapped oil, and water. FTIR results of the deepest deposit demonstrated that mainly sulfur-oxidized compounds are associated with the polar

(61) Mikula, R. J.; Axelson, D. E.; Sheeran, D. Mineral Matter and Clay−Organic Complexes in Oil Sands Extraction Processes. *Fuel Sci. Technol. Int.* **1993**, *11*, 1695−1729.

(62) Kokal, S.; Al-Juraid, J. Quantification of Various Factors Affecting Emulsion Stability: Watercut, Temperature, Shear, Asphaltene Content, Demulsifier Dosage and Mixing Different Crudes. *SPE Paper 56641*, **1999**.

(63) Buckley, J.; Liu, Y.; Monsterieet, S. Mechanisms of Wetting Alteration by Crude Oils. *SPE Paper 37230*, **1997**.

(64) Buckley, J. S.; Liu, Y. Some Mechanisms of Crude Oil/Brine/Solid Interactions. *J. Pet. Sci. Eng.* **1998**, *20*, 155−160.

(65) Batina, N.; Manzano-Martinez, J. C.; Andersen, S. I.; Lira-Galaena, C. AFM Characterization of Organic Deposits on Metal Substrates from Mexican Crude Oils. *Energy Fuels* **2003**, *17*, 532−542.

aggregates. Considering that XANES data identified a marked shift in relative abundance of sulfur species toward oxidized forms at shallower deposits, the relative amount of polar type aggregates could be expected to increase as well. Correspondingly, the inorganic particles decrease in size at shallower deposits along the deposit depth profile. In addition to the demonstrated association of polar or asphaltene type aggregates with carbonate particles, there are indications of formation of clay−organic complexes associated also only with the polar type aggregates.

Summary and Conclusions

A set of synchrotron-radiation-based microanalytical techniques has been applied to investigate depth profile and heterogeneity of organic compounds and metals in a series of deposit samples formed at different depths in blocked tubing strings from an operational oil well. The techniques allow nondestructive investigation of the deposit samples without preliminary treatment (e.g., dissolution, fractionation, centrifugation) commonly needed as sample preparation for many traditional methods. The results indicate the importance of organic−inorganic interactions in deposit formation, the variability in properties and composition of the deposit solids depth profile in the same well, and provide indications regarding aggregate and cluster formation in the deposits. Within the same deposit sample, three different types of aggregates (10−60 μm in size) are identified: predominantly nonpolar, predominantly polar, and nonpolar/polar. The polar aggregates show compositional characteristics consistent with "asphaltene" type aggregates and are shown to be associated with inorganic particles (carbonate and/or clays from the producing formation/drilling muds). The compositional characteristics of the nonpolar aggregates are consistent with "wax" type aggregates. In addition, mixed polar/nonpolar aggregates are observed in the same deposit. Spatial heterogeneity in the metals distribution is found on a scale of several hundred micrometers within the same sample. Heterogeneity in the metal distribution of the deposits is observed with increasing depth, most likely reflecting a systematic change in proportions between the metal distributions associated with decreasing organic and increasing inorganic phases.

The study demonstrates the benefits of applying a set of synchrotron-based techniques for microanalysis and the complementary information provided by XRF, FTIR, and K-edge sulfur XANES. Visualization, compositiona-mapping, high-resolution, and nondestructive analysis of samples are some of the main advantages of applying synchrotron-based microanalytical techniques. The scale of information provided by these microanalytical techniques is applicable to studying organic solid aggregation and petroleum deposition problems as well as in devising and testing the efficiency of chemical and microbial methods for in-situ removal of solid petroleum deposits. Surfactants and chelators could be specifically tailored to the dissolution of the predominant types of organic compounds along the depth profile of the deposits. The application of chemical agents could be combined with use of thermophilic bacteria modified with bioengineering techniques to efficiently consume the specific organic compounds found in oil-well tubing. We suggest a further laboratory investigation of aggregation phenomena and chemical/microbial solid deposit removal methods that could be coupled with a well-constrained field case study.

Acknowledgment. This work was supported in part under U.S. Department of Energy Contract No. DE-AC02-98CH10886.

EF030108A